

Engineering Solid-State Fluorescent Carbon Dots with Aggregation-Induced Emission by Fatty Amine Chains-Regulated Charge Transfer and π - π Stacking

Canpu Yang, Jiusheng Hu, Wenjiang Tan,* Jinhai Si, and Xun Hou

Carbon dots (CDs) are an encouraging green luminescent material; however, the aggregation-caused quenching (ACQ) effect poses a significant limitation for their use in solid-state devices. By adjusting precursor fatty amine chains, this paper synthesized four solid-state emissive CDs with aggregation-induced emission (AIE) properties (Lx-CDs). When water is introduced, the generation of Lx-CDs aggregates creates the switching off of the carbon-core emission (blue) in acetic acid solution and the switching on of the surface-state emission (orange). Results demonstrate that the disulfide bond and fatty amine chain structures allow considerable inhibition in the distance of aromatic skeletons, causing the aggregation-state emission, and the multiple interactions in aggregates can reduce the non-radiative processes benefiting the AIE. Besides, the fast and slow fluorescence species can be confirmed to correspond to the emission paths of carbon-core and surface-state, respectively. The solid-state emission wavelength, photoluminescence quantum yield (PLQY), and AIE strength can be engineered by the fatty amine chain regulated charge transfer and π - π stacking. This study not only reveals the intrinsic mechanism of carbon-core and surface-state luminescence dynamics in AIE CDs but also provides a method for controlling fluorescence wavelength and enhancing the emission of aggregated particles using precursor fatty amine chain length.

1. Introduction

Electroluminescent light-emitting diodes (LEDs) carry a significant function in the display field because of the large color span, excellent operation performance, and superior display contrast. However, the most popular perovskite-based and quantum dots-based LEDs have obvious shortcomings because of the poor environmental effect (heavy metal pollution), which caused unrealistic applications in the commercialization process. Thus, it is

C. Yang, J. Hu, W. Tan, J. Si, X. Hou

Key Laboratory for Physical Electronics and Devices of the Ministry of Education and Shaanxi Key Lab of Information Photonic Technique School of Electronics and Information Engineering

Xi'an Jiaotong University Xi'an 710049, China

E-mail: tanwenjiang@mail.xjtu.edu.cn

The ORCID identification number(s) for the author(s) of this article can be found under https://doi.org/10.1002/adom.202402638

DOI: 10.1002/adom.202402638

necessary to explore environmentally friendly luminescent materials with minimal toxicity and stable permanence immediately. Carbon dots (CDs) with simple preparation and purification, outstanding biocompatibility, and flexible optical characteristics have come to the attention of researchers.[1-10] Currently, researchers have achieved superior photoluminescence quantum yield (PLQY) and variable emission wavelength from ultraviolet to near-infrared.[11-18] In addition, the luminescence mechanism of CDs can be mainly divided into carbon-core state luminescence.[19-21] surface-state luminescence,[22–27] and crosslinking enhancement effect luminescence, [28,29] which have been proven by experiments and theoretical calculations.

Although significant progress in the research of CDs has been gained persistently, the current situation is still unsatisfactory since the stated device performance suffers from the critical aggregation-caused quenching (ACQ) phenomenon, especially in the solid state. The ACQ effect is commonly cited in CDs due to the existence

of some non-radiative processes, including energy transfer and π - π interaction between particles.^[30–32] To overcome this dilemma, some researchers doped CDs as macromolecules and frequently constructed a host-guest system to inhibit the ACQ phenomenon.[33,34] Nonetheless, concentration quenching in CDs can still occur even under this condition. Furthermore, a prevalent issue with many reported CDs is their limited solubility in non-polar organic solvents, posing solubility and compatibility challenges when incorporated into host-guest systems. Additionally, the emission originating from host materials frequently results from an uneven distribution of energy transfer and carrier injection, consequently broadening the electroluminescence spectral bandwidth and compromising the color purity of the fabricated devices. Another viable approach involves introducing steric between CD particles by attaching long-chain structures to their outer surfaces. This strategic modification maintains a suitable distance between the particles, thereby minimizing their interactions and facilitating the achievement of solid-state emission.[35-37] Incorporating such structural modifications, while beneficial, inevitably escalates the synthesis costs and can alter specific inherent properties of the CDs. More critically, it

ADVANCED
OPTICAL
MATERIALS

21951071, 205.2, 7, Downondodd from https://dwarced.onlinelibrary.wiely.com/doi/10.1002/adom.2024/02638 by CAS-XIAN INSTITUTION OPTICS PRECISION MECHANICS, Wiley Online Library of 09/11/2025], See the Terms and Conditions (https://onlinelibrary.wiely.com/terms-and-conditions) on Wiley Online Library for rules of use, O, Aarticles are goverend by the applicable Creative Commons Licenses

imposes constraints on the doping concentration of CDs, and attempts at higher loading fractions are met with a substantial reduction in the PLQY, further highlighting the challenge. Consequently, to fabricate high-performance, monochromatic devices based on CDs, it is paramount to produce CDs with exceptional solid-state emissive properties and utilize them effectively as singular emissive layer components in the LED design.

Since the breakthrough of the aggregation-induced emission (AIE) property by Luo and Tang et al., [38] AIE materials have proven invaluable in solid-state emission applications, with this research group demonstrating that the strategic design of molecular structures can ingeniously yield fluorescent materials exhibiting AIE characteristics, effectively surmounting the challenge posed by the ACQ effect. In addition, AIE materials have found applications in a wide range of fields thanks to their distinctive luminescence, including organic chemical and biological sensing, biological imaging probes, LEDs, lasing, and others.[39-41] It contains small organic molecules and was frequently utilized in metal complexes and semiconductor quantum dots for building solid-state emission samples with exceptional properties.[42,43] The AIE method's advantages can be found in its specific constructional properties, strong link of arrangement performance, and remarkable and tunable solid-state emission characteristics that can be achieved through material construction regulation.[44,45] Iwai et al.[46] reported a series of AIE emitters based on the theoretical prediction of non-radiative decay. They exhibit different quantum yields depending on the alkyl chain length, and the BPST has been reported to have excellent AIE behavior. Yu et al. [47] found that the TPE molecule was more restricted when the carbon chain length increased, resulting in more significant motion restriction, contributing to stronger emissions. The maximum PLQY of complex S4 was 81.37%. Applying the AIE mechanism to the field of CDs and guiding the synthesis of solid-state luminescent CDs was highly promising. Yang et al. [48] found that the formation of H-CD clusters leads to the closure of blue emission as the carbon-core undergoes π - π stacking interactions, and red fluorescence was turned on due to the restriction of intramolecular rotation around disulfide bonds on the surface-state, consistent with the AIE phenomenon. Further, researchers were attempting to introduce the chain length regulation strategies for AIE molecules into the field of CDs, which can achieve effective luminescence in solid-state CD configurations. Xu et al. [49] reported that increased C=N content leads to push-pull electron interactions between the dual fluorescent groups on the CD surface, determining the charge transfer between the dual emissions. As the C=N content increased from 35.6% to 58.4%, the charge transfer efficiency increased from 8.71% to 45.94%, and the fluorescence of CD changed from green to red. An et al.^[50] increased the PLQY of CDs from 19% to 22% by increasing the alkyl chain length of the reaction solvent (amine solvent). However, the basic mechanism of aggregated luminescence is still poorly understood, and achieving effective control over the emission of aggregated particles remains a major challenge, limiting the progress of CDs in more complex applications.[51]

This paper prepared the four solid-state emissive CDs by adjusting precursor fatty amine chains. One confirmed that the fluorescence behavior of the synthesis CDs was dominated by the surface chromophores in the solid state and the intrinsic state in

the solution state by varying the excitation wavelength photoluminescence (PL). The time-resolved photoluminescence (TRPL) of Lx-CDs was explored by time-correlated single photon counting (TCSPC) technology and attributing the two components of fluorescence lifetime to the radiative transition of carbon-core and the surface chromophore, respectively. Besides, the fluorescence of CDs changes from blue to orange with the increase of poor solvents, proving the existence of the AIE. More importantly, the quantum calculation and molecular dynamics simulation were employed to study the solid-state luminescence mechanism with AIE property, i.e., the geometric structures, frontier molecular orbitals, energy levels, excited state properties, fluorescence spectra, electrostatic potential (ESP), the interaction in aggregates, charge transfer processes and the π - π stacking in Lx-CDs. This work elucidates in depth the mechanism of carbon-core and surface-state luminescence in AIE CDs, revealing the chain length-regulated charge transfer and π - π stacking can engineer the solid-state emission wavelength, PLQY, and AIE strength in CDs. It will expedite the progress of seeking efficient CDs material to elevate the efficiency of LEDs.

2. Results and Discussion

2.1. Preparation and Characterization of the Lx-CDs

To prepare high-quality CDs, under the principle of a single variable, one focuses on L5-CDs as the research object to study the various process parameters for preparing Lx-CDs, including molecular molar ratio, heating temperature, and heating time. The molecular molar ratio between reactants (DTSA and 1,5diaminopentane) was first studied. The other experimental conditions remained consistent (hydrothermal kettle with a specification of 50 mL, heated in a blast drying oven at a temperature of 180 °C, heated for 10 h). As shown in Figure S1 (Supporting Information), when the molar ratio of DTSA to 1,5-diaminopentane was 1:1, the steady-state fluorescence intensity of L5-CDs powder reached its maximum value. Heating temperature often has a significant impact on hydrothermal reactions. Therefore, to determine the optimal heating temperature, corresponding powders were prepared under heating temperatures of 160 °C, 180 °C, and 200 °C, respectively, and the other experimental conditions remained consistent (see Figure S2 (Supporting Information)). When the heating temperature was 180 °C, the steady-state fluorescence intensity of the powder reached its maximum value. To further determine the optimal heating time, corresponding powders were prepared for 8 h, 10 h, and 12 h, respectively. They maintained consistency in other experimental conditions during the research process. When the heating time was 10 hours, the steady-state fluorescence intensity of the powder reached its maximum value (see Figure \$3 (Supporting Information)).

In this paper, DTSA-based solid-state emissive Lx-CDs were prepared through a solvothermal reaction at optimal conditions of molar ratio 1:1, 10 h, 180 °C, as schematically displayed in Figure 1. Following the purification steps, an orange appearance color was gained in solid powders (see Figure 1). Notably, when these powders are exposed to ultraviolet light at 365 nm, they display vivid orange PL, suggesting their solid-state emissive property. The as-prepared Lx-CDs have been characterized with TEM, XRD, XPS, and FT-IR to confirm the nature of the

21951071, 2025, 7, Downloaded from https://advancec

com/doi/10.1002/adom.202402638 by CAS-XIAN INSTITUTION OPTICS PRECISION MECHANICS, Wiley Online Library on [09/11/2025]. See the Terms and Conditions (https:

and-conditions) on Wiley Online Library for rules of use; OA articles are governed by the applicable Creative Commons License

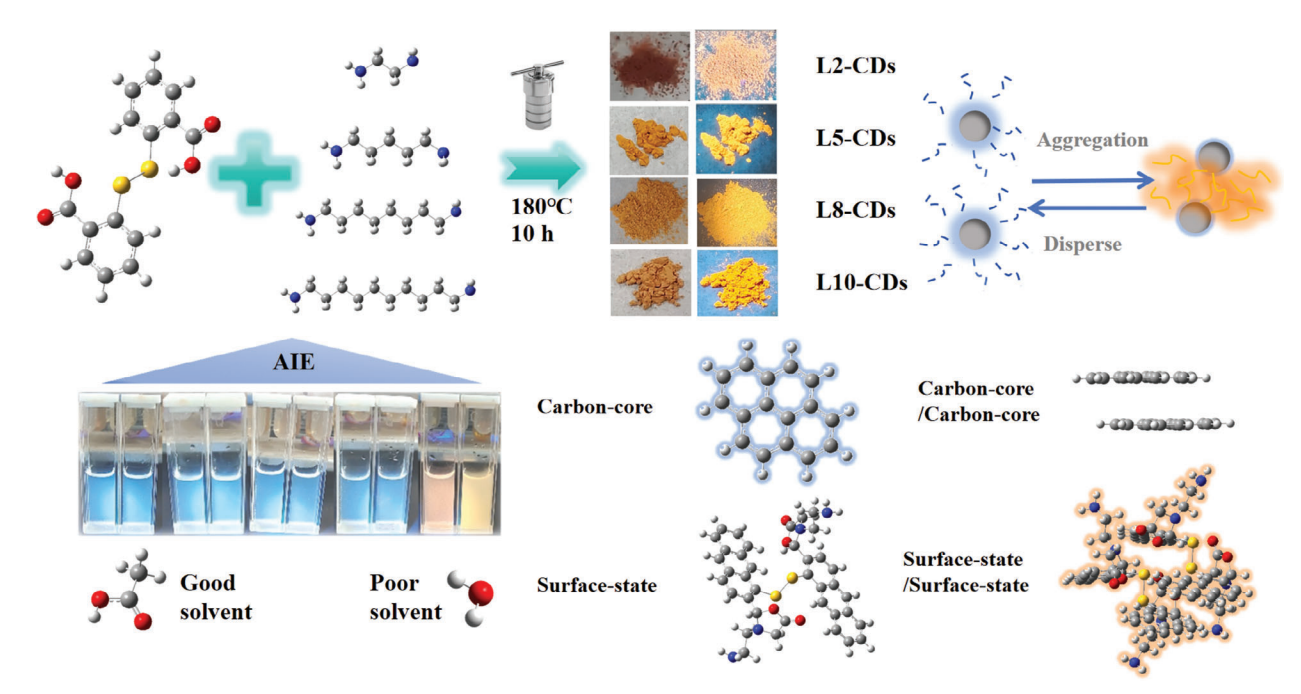


Figure 1. Synthesis and AIE characterization of solid-state emission Lx-CDs; photographs of Lx-CDs under daylight (left) and 365 nm UV light (right); the simulated molecular models for L2-CDs.

carbon nanoparticles. **Figure 2a–d** presents TEM images illustrating the excellent dispersion of the samples, showcasing a consistent average particle diameter (further emphasized in the inset image). The particle size distribution for Lx-CDs was mainly concentrated within the ranges of 2.0-6.0 nm, culminating in a mean particle size measurement of 4–5 nm. The high-resolution TEM (HRTEM) imagery within the inset highlights the presence of unmistakable, sharply defined lattice fringes across all Lx-CDs, measuring 0.21 nm in interval. This spacing corresponds precisely to the (100) crystallographic plane of graphene, testifying to the uniform structural integrity of the CDs. [52–54]

As depicted in Figure \$4 (Supporting Information), the XRD patterns of the Lx-CDs show a prominent, broad peak centered ≈25 degrees, accompanied by less intense peaks at roughly 40 degrees. This broad peak signifies the presence of amorphous carbon, characteristic of an interlayer distance of 0.34 nm. Meanwhile, the faint peak at 40 degrees indicates the (100) crystal plane featuring an interlayer spacing of 0.21 nm.[55-57] The FT-IR spectra for the Lx-CDs were depicted in Figure 2e, demonstrating that due to the similarity in their precursor architectures, these CDs share comparable varieties and intensities of functional groups. One confirmed the presence of methylene (2876 cm⁻¹), [58] amide carbonyl (1676 cm⁻¹), C-N (1413 cm^{-1}) , [59] aromatic C-NH (1260 cm^{-1}) , [60] C-C (1451 cm^{-1}) , C-O (1123 cm⁻¹), S-S (550 cm⁻¹), and C-S (736 cm⁻¹) functional groups or chemical bonds on the surface-state of Lx-CDs. FT-IR spectroscopy also showed that after acylation and carbonization, hydrophilic groups such as hydroxyl (3001 cm⁻¹) and amino (3452 cm⁻¹) were significantly reduced in Lx-CDs, which contributed to the hydrophobicity of Lx-CDs. Previous research has demonstrated that the S-S linkage exhibits a non-rigid structure, allowing the CDs' surface to rotate around it.[48,61] It has been observed that surface molecules on CDs that undergo con-

straints imposed by intramolecular rotation exhibit the AIE phenomenon. In addition, S-S may prevent the quenched fluorescence in the solid state, so the distance between aggregated molecules is crucial. Figure 2f provides a comprehensive XPS survey, confirming the presence of four elemental constituents: carbon (C), nitrogen (N), oxygen (O), and sulfur (S) within the Lx-CD powders. It can be seen that the C element content in the Lx-CDs series samples was as follows: L2-CDs (71.68%), L5-CDs (73.09%), L8-CDs (79.98%), and L10-CDs (81.40%). As the precursor fatty amine increases, the C element in Lx-CDs samples also gradually increases. Specifically, the high-resolution C1s XPS spectrum was further deconvoluted into three distinct Gaussian peaks, as illustrated in Figure S5 (Supporting Information), which were attributed to (C-C/C=C, 56.27% for L2-CDs, 56.77% for L5-CDs, 60.39% for L8-CDs, 61.56% for L10-CDs), (C-N/C-O/C-S, 32.41% for L2-CDs, 34.55% for L5-CDs, 29.44% for L8-CDs, 33.47% for L10-CDs), (C=O, 8.25% for L2-CDs, 8.68% for L5-CDs, 7.57% for L8-CDs, 3.65% for L10-CDs), respectively. The S 2p band (Figure S6 (Supporting Information)) could be split into S-C (56.46% for L2-CDs, 65.28% for L5-CDs, 58.59% for L8-CDs, and 63.53% for L10-CDs), and S-S (19.6% for L2-CDs, 11.85% for L5-CDs, 20.61% for L8-CDs, 9.94% for L10-CDs), which is the essential chemical bond for the solid-state emission with AIE phenomenon in Lx-CDs series samples.

2.2. Optical Properties of the Lx-CDs

The UV-Visible (UV-Vis) absorption, PL excitation, and emission properties of the freshly prepared Lx-CDs in solution and their powdered form were investigated to assess their optical characteristics. As illustrated in Figure S7 (Supporting Information), the UV-Vis absorption spectra of the Lx-CDs dissolved in acetic

21951071, 2025, 7, Downloaded from https://adv

om/doi/10.1002/adom.202402638 by CAS-XIAN INSTITUTION OPTICS PRECISION MECHANICS, Wiley Online Library on [09/11/2025]. See the Term

on Wiley Online Library for rules of use; OA articles are governed by the applicable Creative Commons License

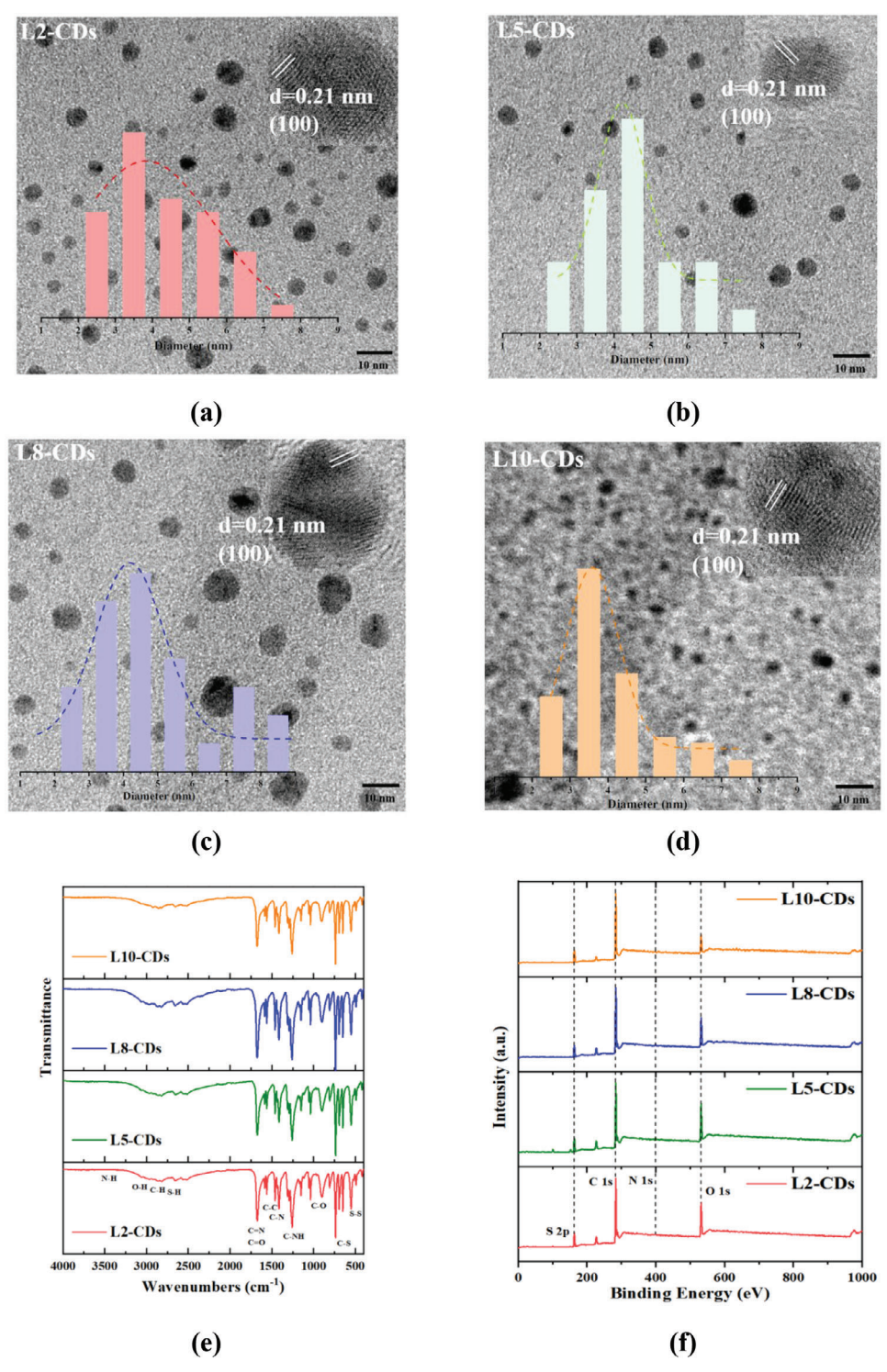


Figure 2. a-d) Inserts present the corresponding high-resolution TEMs and size distribution diagrams of Lx-CDs. e) FTIR spectra; f) XPS spectra.

acid consistently exhibit dual peaks occurring at $\lambda_{\rm max1} \approx 260$ nm and $\lambda_{\rm max2} \approx 320$ nm. These peaks were attributed to the π - π * electronic transitions within the C=C bonds of the carbon-core. The PL emission of Lx-CDs behaves at peaks \approx 460 nm, attributed to the emission of carbon-core state. The Lx-CDs powders exhibited broad PL excitation spectra and different emission peak po-

sitions from the dispersed state (*see* **Figure 3**). An excitation signal of \approx 460 nm corresponds to a fluorescence emission peak of \approx 490 nm, and an excitation signal of \approx 550 nm corresponds to a fluorescence emission peak of \approx 600 nm. For L2-CDs, the $\lambda_{\rm max1}$ was located at 478 nm, and the $\lambda_{\rm max2}$ was located at 580 nm; for L5-CDs, the $\lambda_{\rm max1}$ was located at 492 nm, and the $\lambda_{\rm max2}$ was

21951071, 2025, 7, Downloaded from https://adv

doi/10.1002/adom.202402638 by CAS-XIAN INSTITUTION OPTICS PRECISION MECHANICS, Wiley Online Library on [09/11/2025]. See the Term

litions) on Wiley Online Library for rules of use; OA articles are governed by the applicable Creative Commons License

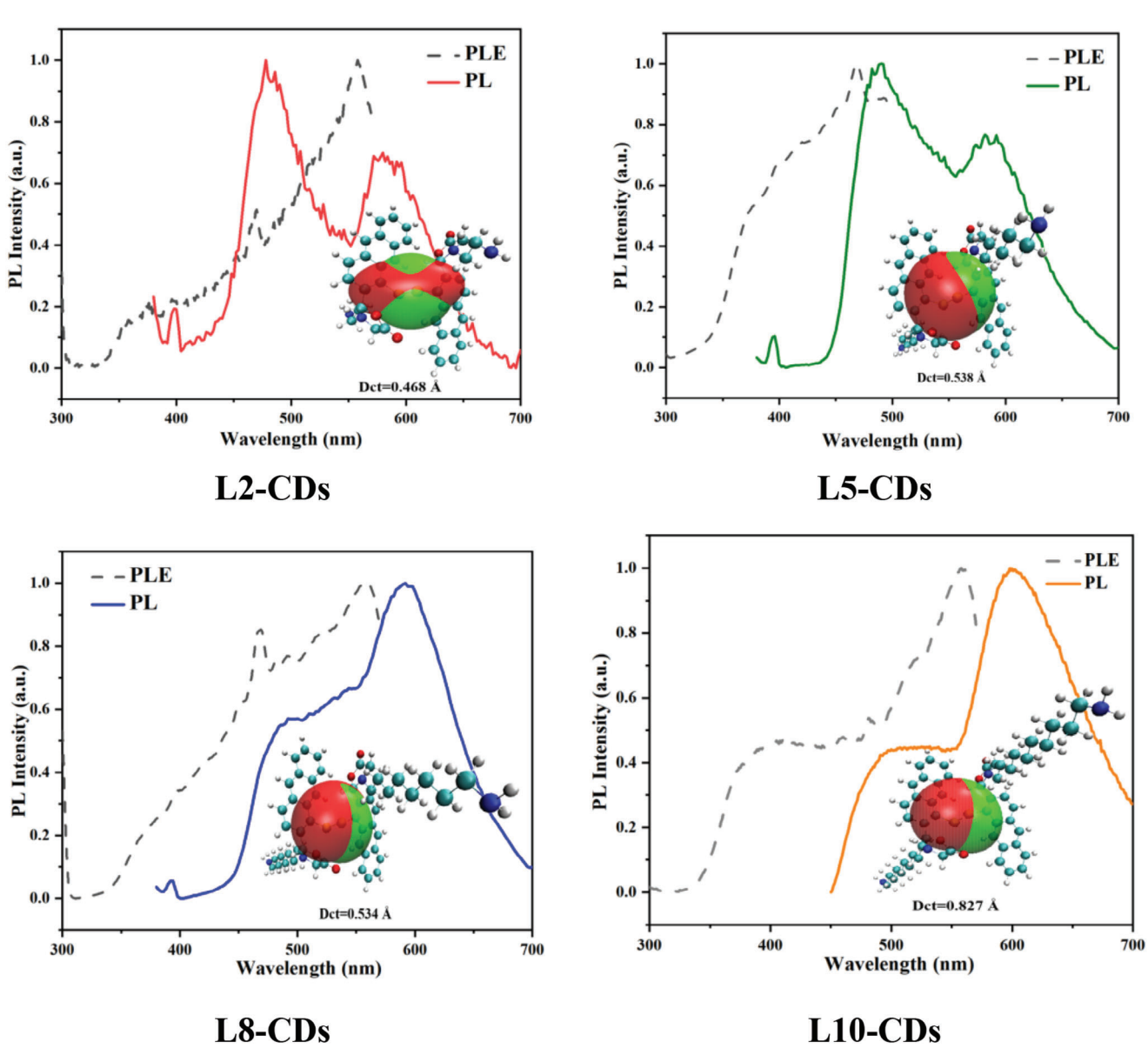


Figure 3. PL excitation (grey line) and PL emission (multicolor line) of Lx-CDs. Insets: the charge transfer distance (Dct) of hole centroids (green) and electron centroids (red) on excitation of Lx-CDs.

located at 592 nm; for L8-CDs, the $\lambda_{\rm max1}$ was located at 490 nm, and the $\lambda_{\rm max2}$ was located at 590 nm; for L10-CDs, the $\lambda_{\rm max1}$ was located at 500 nm, and the $\lambda_{\rm max2}$ was located at 600 nm. When focused on the $\lambda_{\rm max2}$, a red-shifted peak from 580 nm (L2-CDs) to 592 nm (L5-CDs), a similar peak at 592 nm for L5-CDs and 590 nm for L8-CDs, and follows a red-shifted peak from 590 nm (L8-CDs) to 600 nm (L10-CDs), which may relate to the charge transfer state.

Further, the variable excitation spectra of Lx-CDs in solution and powder have been studied to demonstrate the attribution of emission peaks in Figure S8 (Supporting Information). When Lx-CDs are dispersed in an acetic acid solution, their fluorescence emission spectra exhibit excitation wavelength-dependent characteristics, and the intrinsic emission from the carbon-core is primarily determined by size effects. Consequently, it can be

Adv. Optical Mater. 2025, 13, 2402638

reasonably inferred that the fluorescence signal of Lx-CDs in the dispersed state at $\approx\!460$ nm should come from the intrinsic emission of the carbon-core. In addition, the fluorescence emission peak of Lx-CDs powders hardly changes with the excitation wavelength, which means the fluorescence signal of Lx-CDs in the powder state mainly comes from the surface chromophores. In addition, PLQY is an essential indicator for measuring optical materials. As shown in Figure S9 (Supporting Information), one conducted absolute fluorescence quantum efficiency tests on Lx-CDs with the value of L10-CDs (5.90%) > L5-CDs (4.28%) > L8-CDs (3.91%) > L2-CDs (3.04%). As the precursor fatty amine chain length increases, the PLQY of Lx-CDs powder also increases. Still, there is an abnormal phenomenon between L5-CDs and L8-CDs; specific analysis will be discussed later.

21951071, 2025, 7, Downloaded from https://advanced

om/doi/10.1002/adom.202402638 by CAS-XIAN INSTITUTION OPTICS PRECISION MECHANICS, Wiley Online Library on [09/11/2025]. See the Terms

on Wiley Online Library for rules of use; OA articles are governed by the applicable Creative Commons License

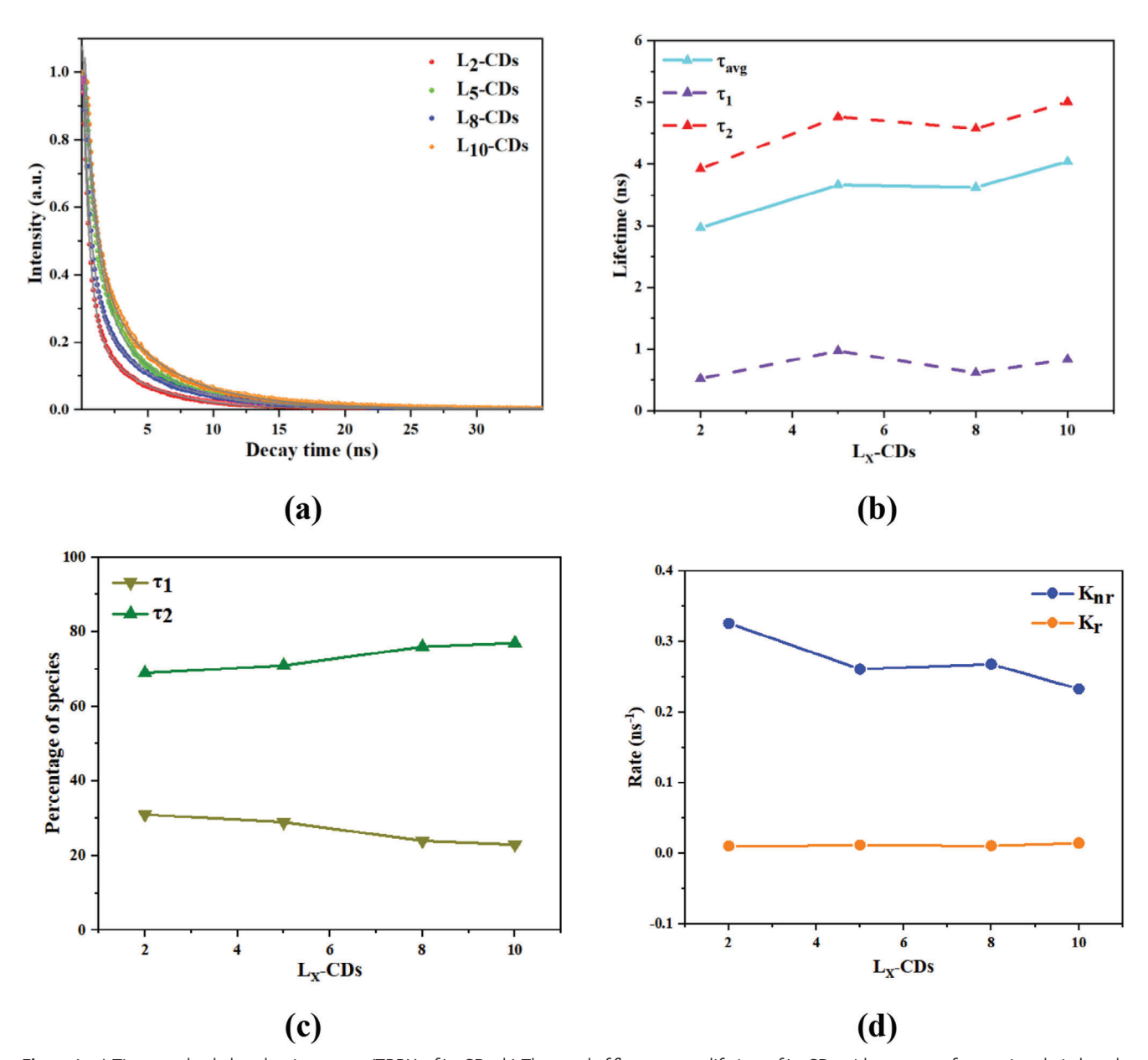


Figure 4. a) Time-resolved photoluminescence (TRPL) of Lx-CDs. b) The trend of fluorescence lifetime of Lx-CDs with precursor fatty amine chain length. c) The trend of the proportion of fast and slow species. d) non-radiative coefficient K_{nr} and radiative coefficient K_r during the fluorescence lifetime decay process of Lx-CDs.

2.3. Fluorescence Lifetime Decay Curves of Lx-CDs

Adv. Optical Mater. 2025, 13, 2402638

The characteristics of the fluorescence lifetime decay curves of Lx-CDs powder samples are shown in **Figure 4a**. Further, one performed double exponential fitting on the fluorescence lifetime decay curves of Lx-CDs by the following equations, and the specific fitting data were shown in Table S1 (Supporting Information).

$$I(t) = A_1 \exp\left(-\frac{t}{\tau_1}\right) + A_2 \exp\left(-\frac{t}{\tau_2}\right) \tag{1}$$

$$\tau_{avg} = \frac{A_1 \tau_1^2 + A_2 \tau_2^2}{A_1 \tau_1 + A_2 \tau_2} \tag{2}$$

In this scenario, τ_1 and τ_2 signify the decay time constants, while A_1 and A_2 denote the pre-exponential factors associated with the respective decay lifetimes of τ_1 and τ_2 . The lifetime-weighted fractional intensities P_1 (%) and P_2 (%) are derived through a weighted calculation based on A_1 and A_2 , reflecting the relative intensity contributions of each component in the double exponential fitting process. The average lifetimes (τ_{avg}) in Figure 4b behaved in the order as follows: L10-CDs (4.04 ns) > L5-CDs (3.66 ns) > L8-CDs (3.62 ns) > L2-CDs (2.97 ns), which

___ MATERIALS

21951071, 2025, 7, Downloaded from https://advanced.onlinelibrary.wiley.com/doi/10.1002/adom.202402638 by CAS-XIAN INSTITUTION OPTICS PRECISION MECHANICS, Wiley Online Library on [09/11/2025]. See the Terms and Conditions (https://advanced.onlinelibrary.wiley.com/doi/10.1002/adom.202402638 by CAS-XIAN INSTITUTION OPTICS PRECISION MECHANICS, Wiley Online Library on [09/11/2025]. See the Terms and Conditions (https://advanced.onlinelibrary.wiley.com/doi/10.1002/adom.202402638 by CAS-XIAN INSTITUTION OPTICS PRECISION MECHANICS, Wiley Online Library on [09/11/2025]. See the Terms and Conditions (https://advanced.onlinelibrary.wiley.com/doi/10.1002/adom.202402638 by CAS-XIAN INSTITUTION OPTICS PRECISION MECHANICS, Wiley Online Library on [09/11/2025]. See the Terms and Conditions (https://advanced.onlinelibrary.wiley.com/doi/10.1002/adom.202402638 by CAS-XIAN INSTITUTION OPTICS PRECISION MECHANICS, Wiley Online Library on [09/11/2025]. See the Terms and Conditions (https://advanced.onlinelibrary.wiley.com/doi/10.1002/adom.202402638 by CAS-XIAN INSTITUTION OPTICS PRECISION MECHANICS.

and-conditions) on Wiley Online Library for rules of use; OA articles are governed by the applicable Creative Commons License

was consistent with the order of PLQY values. The fluorescence lifetime of Lx-CDs powder can be resolved into two fluorescence radiation processes: (1) Fast process (τ_1): carrier transition from carbon-core undergo radiative recombination transitions directly to the ground state and emitting photons; (2) Slow process (τ_2): Carriers first transfer from carbon-core to the surface-state and the surface-state undergoes radiative recombination transition to the ground state and emitting photons. Interestingly, it can be seen that during the fluorescence delay process of Lx-CDs, the proportion of fast processes monotonically decreases (from 31% of L2-CDs to 23% of L10-CDs). In comparison, the proportion of slow processes in the opposite direction monotonically increases (from 69% of L2-CDs to 77% of L10-CDs) (see Figure 4c). This phenomenon indicated that the ratio of slow to fast processes monotonously increases as the precursor fatty amine chains rise, indicating that the surface molecules can more effectively radiate photons. When it comes to the value of τ_2 , it has the order of L10-CDs (5.009 ns) > L5-CDs (4.764 ns) > L8-CDs (4.575 ns) > L2-CDs (3.923 ns), which shows although L8-CDs has a higher proportion of surface-state emission than L5-CDs, the lower τ_2 in L8-CDs suggests an undesirable process of non-radiative recombination in surface-state.

To gain a deeper understanding of the physical mechanisms in Lx-CDs, the K_r (radiation decay rate) and K_{nr} (non-radiation decay rate) of Lx-CDs in the solid state were calculated according to the following equations:^[62]

$$K_{r} = \frac{PLQY}{\tau} \tag{3}$$

$$K_{nr} = \frac{1 - PLQY}{\tau} \tag{4}$$

The calculated K_r and K_{nr} values are shown in Table S1 (Supporting Information) and Figure 4d. The K_r behave the order of L10-CDs (0.0146 ns⁻¹) > L5-CDs (0.0117 ns⁻¹) > L8-CDs (0.0108 ns⁻¹) > L2-CDs (0.0103 ns⁻¹), and the K_{nr} have the order of L10-CDs (0.233 ns⁻¹) < L5-CDs (0.261 ns⁻¹) < L8-CDs (0.268 ns⁻¹) < L2-CDs (0.326 ns⁻¹). The above results were consistent with the order of PLQY, indicating that the precursor fatty amine chains simultaneously affect the radiative and nonradiative processes of Lx-CDs. The non-radiative changes were more pronounced, suggesting the generation of the AIE effect, as the long-chain surface-state may effectively limit the nonradiative processes, such as rotation and vibration of surface chromophores.

2.4. AIE Characteristics of Lx-CDs

The sample was dispersed in a series of mixed solutions of poor solvent/good solvent during the preparation of nano sediments. As shown in Figure S10 (Supporting Information), the clear solution on the left side of each plot indicates that Lx-CDs powder can be well dispersed in the acetic acid solvent. In contrast, the turbid solution on the right side of the corresponding plot indicates that Lx-CDs powder cannot be well dispersed in a deionized water solvent. Therefore, acetic acid and deionized water were selected as good and poor solvents for Lx-CDs, respectively. As the proportion of deionized water in the mixed solution increases,

the concentration of Lx-CDs in the acetic acid part of the mixed solution will inevitably increase, forcing Lx-CDs to form nano aggregates. As shown in Figure S11 (Supporting Information), when the proportion of deionized water in the mixed solvent was small (≤70%), the fluorescence of Lx-CDs was mainly dominated by intrinsic emission from the carbon-core, displaying blue fluorescence emission. When the proportion of deionized water exceeds 80%, Lx-CDs form nano aggregates in the mixed solution, and the fluorescence emission of Lx-CDs dominates from surface chromophores, displaying orange fluorescence emission. Further, one investigated the effect of precursor fatty amine chain length on the AIE characteristics of Lx-CDs.

As shown in Figure 5, the grey dashed box represents the fluorescence emission spectrum of Lx-CDs in their dispersed state at their optimal excitation wavelength of 380 nm. In comparison, the red dashed box represents the fluorescence emission spectrum of Lx-CDs at their optimal excitation wavelength of 470 nm when forming nano aggregates. The ratio of the strongest signal value of the fluorescence emission spectrum ≈600 nm in the aggregated state of Lx-CDs to the strongest signal value in the dispersed state of Lx-CDs was defined as the AIE coefficient, with chain length as the reference variable. (see Figure \$12, Supporting Information). The AIE coefficient had the order of L10-CDs (1.18 a.u.) > L5-CDs (1.04 a.u.) > L8-CDs (0.82 a.u.) > L2-CDs (0.34 a.u.), which was consistent with the PLQY values. The weakening of dispersed PL may be due to the fact that in the dispersed state, the surface-state of the long chain may undergo more nonradiative motion. The enhancement of the aggregated-state PL may be attributed to the multiple interactions between surface molecules, which can significantly reduce the non-radiative coefficient.

2.5. Theoretical Calculation

A comprehensive comparison of numerous properties of the four Lx-CDs was conducted, including the effect of precursor fatty amine chain length on optical properties, fluorescence lifetime, PLQY, radiative and non-radiative processes, and AIE characteristics (see Table S2, Supporting Information). One carried out the DFT method to explore the sophisticated fluorescence emission in carbon-core and surface molecules, as shown in Figure 1. The excited state data and simulated fluorescence spectra were shown in Table \$3 and Figure \$13 (Supporting Information). For the simulated fluorescence spectra of Lx-CDs, it can be observed that there were two fluorescence peaks, one located in the blue light range and the other located ≈600 nm, which is consistent with the experimental spectra. The dihedral angles between the various parts of monomer surface molecules were studied, as shown in Figure S14 (Supporting Information). The θ_1 and θ_6 were ≈ 65 – 70 degrees, and the θ_2 and θ_5 were also nonplanar for Lx-CDs surface molecules (SLx-CDs), which means the fatty amine chains may increase the steric hindrance of molecules and the solidstate PL occur. The θ_3 and θ_4 were the dihedral angles between the disulfide bond and the anthracene group; they can be found to exceed 80 degrees, and the nearly vertical configuration was proof that the disulfide bond serves as a solid-state luminescent core group. Molecular ESP explains and predicts active sites. [63–66] As shown in Figure S15 (Supporting Information), it can be seen

21951071, 2025, 7, Downloaded from https://advancec

om/doi/10.1002/adom.202402638 by CAS-XIAN INSTITUTION OPTICS PRECISION MECHANICS, Wiley Online Library on [09/11/2025]. See the Terms

ditions) on Wiley Online Library for rules of use; OA articles are governed by the applicable Creative Commons Licenso

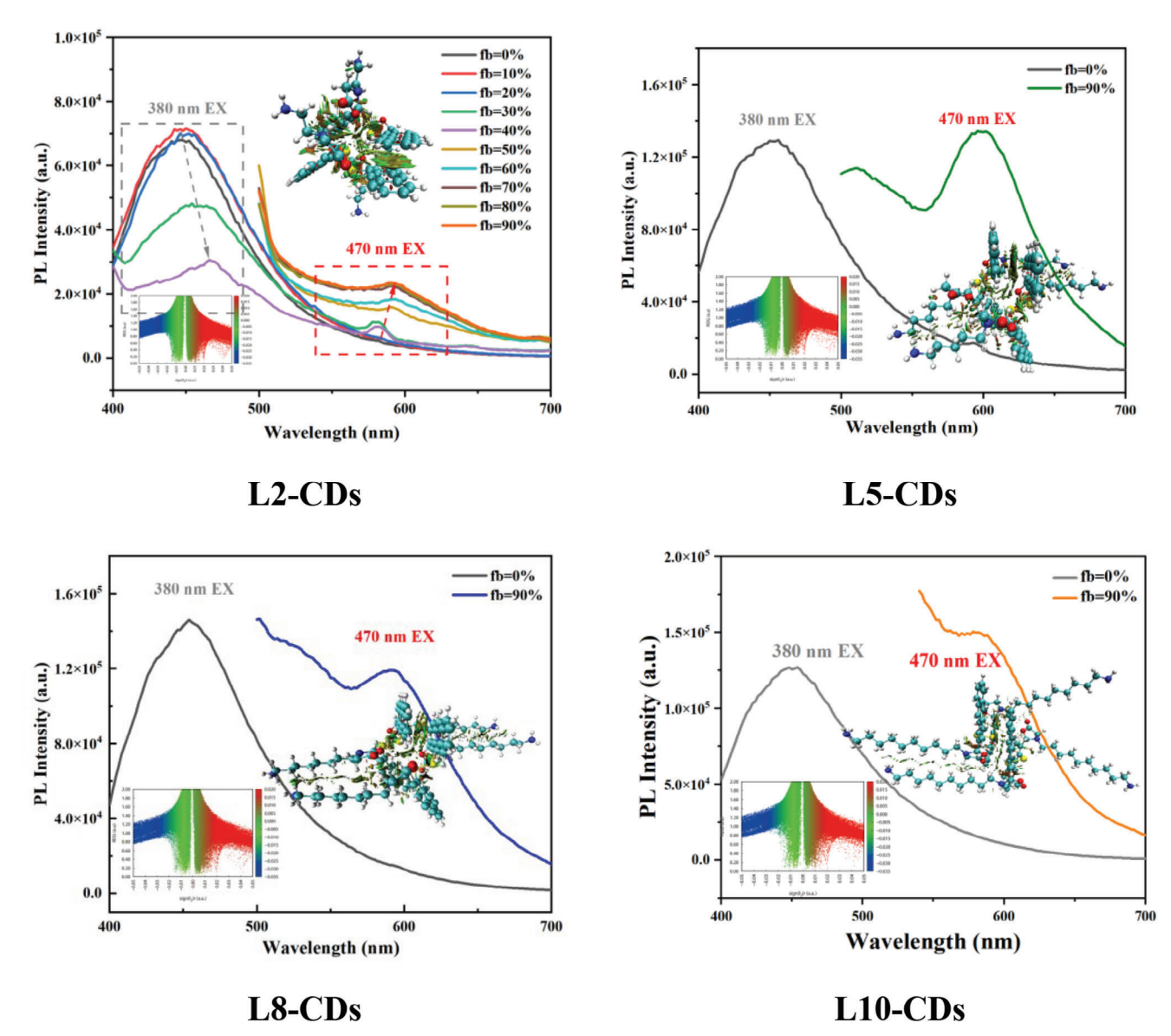


Figure 5. Fluorescence emission spectra (fb: fraction of bad solvent) of Lx-CDs powder dispersed in a mixed solution of 0%–90% water/acetic acid. Insert: Plots of the RDG versus the electron density multiplied by the sign of the second Hessian eigenvalue and gradient isosurfaces of RGD for the aggregates.

that the end of the fatty amine chain in SLx-CDs was the position with the lowest ESP value, and the change in ESP values indicates that the chain length leads to a difference in electrophilic reactions. In addition, the alternating distribution of positive and negative ESP values ensures the formation of aggregates.

The energy level and frontier molecular orbitals (HOMO, LUMO) distribution as intrinsic electronic structures of the molecules can affect the excitation and fluorescence process to a significant extent. [67–69] The HOMO and LUMO energy levels of SLx-CDs behave at similar values at \approx -6.6 eV and -1.2 eV, respectively (see Table S4, Supporting Information). The LUMO energy level of the carbon-core holds the value of -0.33 eV, and the lower LUMO energy levels of surface molecules than the carbon-core make the charge transfer from the carbon-core to surface molecules. Electron spatial distributions of HOMO-

1 to LUMO+1 molecular orbitals of carbon-core and surface molecules were illustrated in Figure S16 (Supporting Information), and the principal contribution of each part was shown in Table S5 (Supporting Information). For the carbon-core, the HOMO and LUMO were provided by the whole aromatic rings. For the surface molecules, the HOMOs represented π -type orbitals, and LUMOs represented π *-type orbitals. Apparently, the HOMOs were mainly contributed by two sides groups (98%), and the LUMOs were distributed not only at the two sides moieties (< 80%) but also at the disulfide bond part (> 20%). Besides, the contribution of the two sides groups to the HOMOs was different, and the SL10-CDs behaved the most average distribution (22%, 76%) compared to the others; For the LUMOs, it was evident that the left group contributed more to LUMOs than the right group. Compared with other CDs, the contribution of the disulfide bond

ADVANCED
OPTICAL
MATERIALS

2195/071, 2025, 7, Downloaded from https://advanced.onlinelibrary.wiley.com/doi/10.1002/adom.2024/02638 by CAS-XIAN INSTITUTION OPTICS PRECISION MECHANICS, Wiley Online Library on [09/11/2025]. See the Terms and Conditions (https://onlinelibrary.wiley.com/terms

and-conditions) on Wiley Online Library for rules of use; OA articles are governed by the applicable Creative Commons License

to LUMO in SL10-CDs (26%) was the largest, and the difference in contribution between the two sides groups to LUMO (53%, 21%) was the smallest. In addition, the different distribution and partial overlap of HOMOs and LUMOs are beneficial for the occurrence of charge transfer.

The charge transfer process is related to the larger distorted structure of the molecule itself and the electron-donating ability of the donor group or the electron-withdrawing ability of the acceptor group.[70,71] With the increase of the electron-donating or electron-withdrawing abilities in the molecular functional groups, the components of the charge transfer state in the mixed excited state increase correspondingly, the transition dipole moment of the excited state increases significantly, and the maximum peak of the absorption and fluorescence emission shows red-shift. The CDD diagrams in the excited state of Lx-CDs surface molecules were shown in Figure S17 (Supporting Information), and the charge transfer distances (Dct) were presented in Figure 3 (Inserts). It can be seen that the electron and hole density were mainly distributed at the disulfide bond and anthracene moiety, and the different chain lengths of fatty amines affect charge configuration. The charge transfer was measured by the distance between the hole density center and the electron density center, and there was a trend as follows: SL10-CDs (0.827 Å) > SL5-CDs (0.538 Å) > SL8-CDs (0.534 Å) > SL2-CDs (0.468 Å). The order of the charge transfer distances is consistent with the order of spectral red-shift, which proves that the maximum fluorescence wavelength of surface-state luminescence is closely related to the performance of charge transfer processes. In addition, the excited state transition dipole moments of SLx-CDs were calculated, as shown in Figure S18 (Supporting Information). SL10-CDs have the maximum excited state transition dipole moment of 2.72 D, attributed to the longest fatty amine chain, suggesting the highest radiative recombination rate. The spontaneous emission rate can be obtained by the reciprocal of the fluorescence lifetime (τ), and the following formula can obtain the simulated fluorescence lifetime:[72]

$$\tau = \frac{ac^3u^2}{2fe^2} \tag{5}$$

where f and e represent the oscillator strength and excitation energy, parameters (a, u) are constants, and e is the light speed. The results calculated by the relationship between K_r and K_{nr} were shown in Figure S19 (Supporting Information), with K_r in the following order: SL10-CDs $(0.047~{\rm ns^{-1}})$ > SL5-CDs $(0.042~{\rm ns^{-1}})$; the K_{nr} follow the trend of SL10-CDs $(0.754~{\rm ns^{-1}})$ < SL5-CDs $(0.934~{\rm ns^{-1}})$ < SL8-CDs $(1.015~{\rm ns^{-1}})$ < SL2-CDs $(1.307~{\rm ns^{-1}})$. It can be seen that SL10-CDs have the highest radiative recombination rate and the lowest non-radiative recombination rate, indicating the enhanced recombination and weakened non-radiative recombination, leading to the highest PLQY value.

Further, it is a crucial aspect of investigating the charge transfer in the carbon-core/surface-state, and the morphologies calculated by molecular dynamics simulations are shown in Figure S20 (Supporting Information). Then, Figure S21 (Supporting Information) displayed the optimized structures of the ground state and frontier molecular orbitals of the carbon-core/SLx-CDs complexes. For the HOMOs of carbon-core/SLx-CDs complexes, charge delocalization occurs on the carbon-core and SLx-CDs,

and it is nearly all concentrated on the SLx-CDs for the LUMOs. In addition, to quantify the specific contributions of carbon-core and SLx-CDs to frontier molecular orbitals, the PDOS were calculated in Table S6 (Supporting Information). The contribution rates of carbon-core to the HOMOs in the four complexes were 43% for carbon-core/SL2-CDs, 37% for carbon-core/SL5-CDs, 45% for carbon-core/SL8-CDs and 43% for carbon-core/SL10-CDs. In contrast, the contribution rates of carbon-core to the LU-MOs in the investigated complexes were 2%, 2%, 1%, and 2%. It implies that the charge transfer direction during excitation is from the carbon-core to the surface-state. Additionally, the CDD of the excited states for the four compounds revealed the function of each group for the charge transfer process (see Figures S22 and S23, Supporting Information), and the excited state data were shown in Table \$7 (Supporting Information). By observing and analyzing each of the CDD from S₁ to S₆, it becomes evident that they fall under three specific classifications as follows: (1) Most electrons and holes were situated on the carbon-core; for instance, S₅ for carbon-core/SLx-CDs, S₆ for carbon-core/SL2-CDs and carbon-core/SL10-CDs, revealing the localized excitation and charge transfer take place mainly at the carbon-core. (2) The holes and electrons were situated on the carbon-core and SLx-CDs in the S₄ excited states, indicating the near-complete charge transfer. (3) For S₁, S₂, and S₃ excited states of carbon-core/SLx-CDs and S_6 of carbon-core/SL5-CDs series, most holes and electrons were distributed on the surface molecules, suggesting that charge transfer occurs merely at the SLx-CDs.

Considering the fragments charge transfer in the carboncore/surface-state complexes, 0.858 e^- , 0.870 e^- , 0.914 e^- , and 0.926 e- charge quantity was transferred from carbon-core to the SL2-CDs, SL5-CDs, SL8-CDs, and SL10-CDs, respectively (see Figure \$24, Supporting Information). Besides, the donoracceptor charge transfer rates are usually estimated using the Marcus theory. [73-75] All parameters related to charge transfer integral (V_{DA}) , [76,77] the reorganization energy (λ) values, and the variations in free energy occurring specifically during the charge transfer processes (ΔG_{CS}) of the carbon-core/SLx-CDs complexes can be calculated in Table S8 (Supporting Information).^[78–80] The estimated charge transfer rates (K_{CS}) for carbon-core/SL2-CDs, carbon-core/SL5-CDs, carbon-core/SL8-CDs, and carboncore/SL10-CDs were $1.0 \times 10^{15} \text{ s}^{-1}$, $1.2 \times 10^{15} \text{ s}^{-1}$, 4.2×10^{15} s^{-1} , and 4.3×10^{15} s⁻¹, respectively. The monotonically increasing charge transfer rate and charge transfer quantity suggested that the increase in fatty amine chains was beneficial for improving surface-state emission.

Further, the π - π stacking in aggregates has a significant impact on surface-state emission. To explain the lower PLQY of L8-CDs compared to L5-CDs in the experiment, one uses molecular dynamics to construct a reasonable stacking configuration (*see* **Figure 6a**), and the crystal structures with the lowest energies were optimized for Lx-CDs. Conjugated systems can form a misaligned parallel arrangement^[81] with a configuration, as shown in Figure S25 (Supporting Information). First, the HOMOs and LUMOs, together with the CDD of the excited states, were illustrated in Figure S26 (Supporting Information). [82] The HOMOs and LUMOs were both distributed by two monomer molecules. This means that the charge transfer process may occur in the aggregates after photoexcitation, improving PL performance. One drew localized orbital locator (LOL) diagrams of carbon-core and

21951071, 2025, 7, Downloaded from https://advanced.onlinelibrary.wiley

com/doi/10.1002/adom.202402638 by CAS-XIAN INSTITUTION OPTICS PRECISION MECHANICS, Wiley Online Library on [09/11/2025]. See the Terms

and-conditions) on Wiley Online Library for rules of use; OA articles are governed by the applicable Creative Commons License

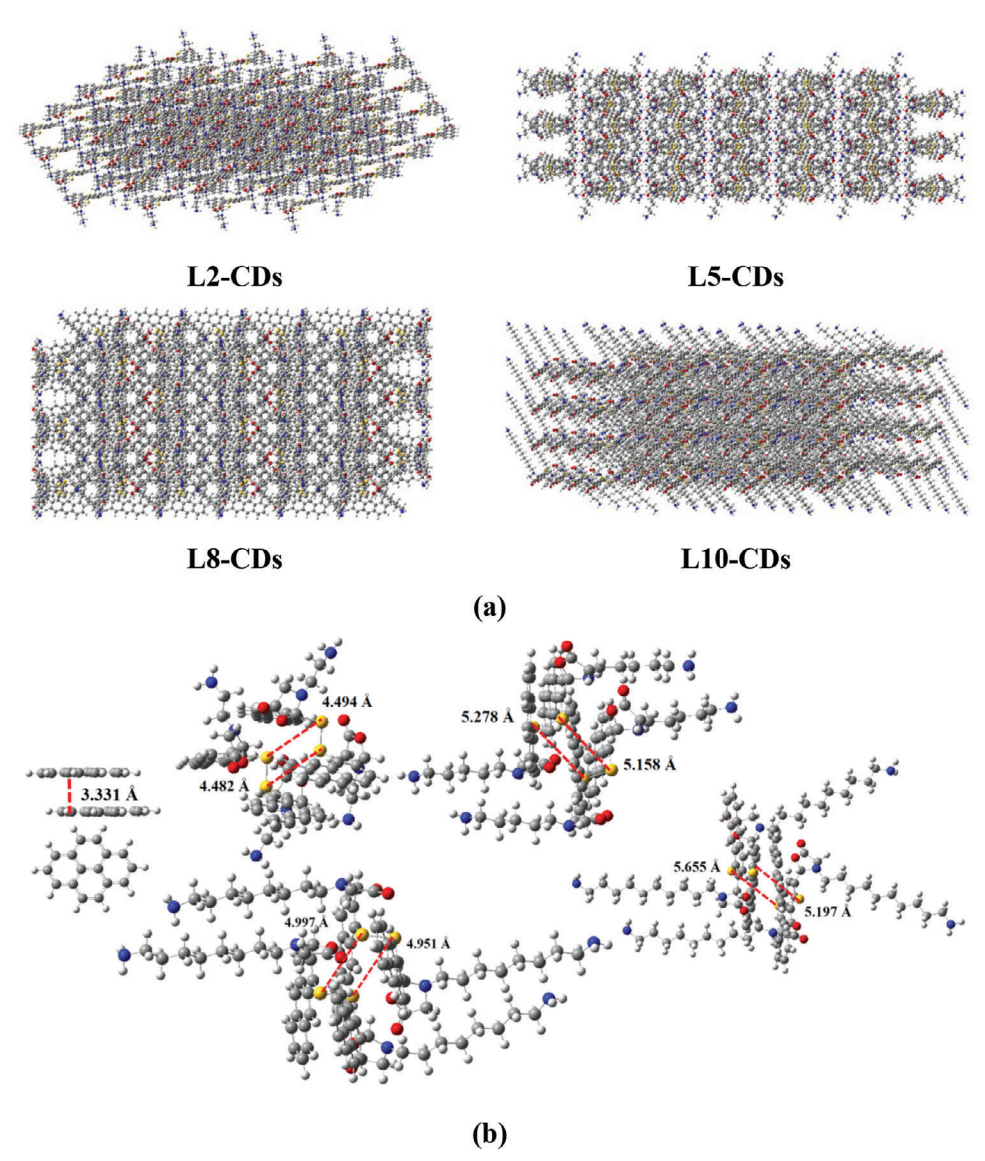


Figure 6. a) The surface-state stacking morphologies extracted from molecular dynamics simulations of Lx-CDs. b) The optimized carbon-core and the surface-state distance (D in Å) reflected the π - π stacking in Lx-CDs aggregates.

surface molecules and calculated the LOLIPOP index^[83] to measure the ability of π - π stacking of the molecules (Figure S27 (Supporting Information)). It can be seen that π electrons were mainly distributed on the benzene ring, and the values of benzene rings at both ends of the carbon-core were 7.82 and 7.7, which indicates that the carbon-core is easier to produce π - π stacking than the surface molecules (LOLIPOP index < 7.2), leading to fluorescence quenching. For the surface molecules, the order of LOLIPOP index was as follows: SL10-CDs (6.95, 6.54, 6.47) < SL5-CDs (6.97, 6.54, 6.50) < SL8-CDs (7.02, 6.61, 6.51) < SL2-CDs (7.11, 6.62, 6.54). The results showed that the π - π stacking of SL8-CDs would increase compared with SL5-CDs, which was not conducive to improving fluorescence lifetime and PLQY. [84]

Further, the visualization of π - π stacking of aggregates (the interaction region indicator images) was shown in Figure S28 (Supporting Information),^[85] and the measured distances between

carbon-core aggregates and the distances between surface-state aggregates were shown in Figure 6b. The distance between aggregates can directly reflect the strength of π - π stacking. It can be seen that the aggregation distance of carbon-core was ≈ 3.3 Å, which leads to the abundant quenching of solid-state carbon-core luminescence. The distances between surface aggregates were all above 4.4 Å, which were attributed to the vertical conformation of disulfide bonds and related to fatty amine chains, leading to solid-state luminescence. The distances of surface-state aggregates were as follows: L10-CDs (5.655 Å, 5.197 Å) > L5-CDs (5.278 Å, 5.158 Å) > L8-CDs (4.997 Å, 4.951 Å) > L2-CDs (4.494 Å,4.482 Å). The distance of surface-state aggregates further proved the more serious π - π stacking of L8-CDs than L5-CDs, consistent with the predicted results of the LOLIPOP index. Interestingly, although the long-lived fluorescence proportion increased monotonically with the increase of the fatty amine chain of the www.advancedsciencenews.com



2195/071, 2025, 7, Downloaded from https://da/vanced.onlinelibrary.viley.com/doi/10.1002/adom.2024/02638 by CAS-XIAN INSTITUTION OPTICS PRECISION MECHANICS, Viley Online Library on [09/11/1025]. See the Terms and Conditions (https://onlinelibrary.viley.com/terms

and-conditions) on Wiley Online Library for rules of use; OA articles are governed by the applicable Creative Commons License.

www.advopticalmat.de

precursor, this result revealed that the decrease of fluorescence lifetime and PLQY in L8-CDs was related to the enhancement of π - π stacking inhibiting the improvement of solid-state luminescence efficiency.

Finally, the AIE performance is related to the non-radiative processes of vibration and rotation of surface-state molecules. One investigates the AIE characteristics of Lx-CDs by studying interactions in aggregates. The x-axis depicts the sign of the second largest eigenvalue of the Hessian matrix of the electron density (λ_2) multiplied by the electron density $(\rho(\mathbf{r}))$, which is sign (λ_2) ρ , was drawn in RDG (see Figure 5 Insert). The weak interactions, including dispersion, occurred in the low-density regions; however, the stronger interactions, such as either stabilizing attractive (λ_2 < 0) or destabilizing repulsive (λ_2 > 0) interactions, were related to the higher density scales. [86] Thus, the strength of interactions can be obtained by analyzing electron density. In contrast, the value of λ_2 was divided into bonded interaction with the negative value and nonbonded interaction with the positive value. The blue area with a negative value of sign(λ_2) ρ showed attractive weak interaction, and the most common one in line with this feature was the hydrogen bond. The red area had the positive value of sign(λ_2) ρ , corresponding to the strong steric effect region in the ring and cage (nonbonded overlap). To determine the situation, a structural representation of the aggregates was created to illustrate the noncovalent interactions present visually. This depiction utilized values of sign(λ_2) ρ ranging from -0.035 to 0.02 au, with the surfaces color-coded on a blue-green-red scale, as shown in Figure 5 (Inserts). It can be seen that the abundance of green and brown isosurfaces corresponds to strong van der Waals interactions and spatial hindrance. In the RDG picture, the number of high-density and low-gradient spikes lying at positive parts verifying the steric energy, and the placement of the low-density and low-gradient region occurred at the positive portions, ensuring the stabilization through an attractive force derived from the dispersion interaction energy. The total interaction energies in Lx-CDs aggregates all had a negative value (absolute value greater than 35 kcal mol⁻¹), demonstrating solid interactions when forming aggregates. Due to multiple interactions at disulfide bonds and fatty amine chains, strong interaction forces resulted in limited vibration of surface-state molecules, reducing non-radiative recombination. Therefore, as the amount of poor solvents increases, the surface-state luminescence is enhanced along with the AIE coefficients.

3. Conclusion

Using molecular amines with different carbon numbers and DTSA as precursors, solid-state emission Lx-CDs with dual emission centers for blue and orange lights were initially synthesized. TRPL technology, quantum calculation, and molecular dynamics simulations were employed to reveal the fluorescence dynamics of CDs. The main results are as follows: (1) The disulfide bonds and fatty amine chain structures allow inhibition in the distance of aromatic skeletons, causing the solid-state emission. (2) The AIE characteristics are attributed to generating various interactions in aggregates, which weakens the non-radiative recombination process. (3) The red-shift of the surface-state emission peak by regulating fatty amine chains is closely related to the charge transfer state, and a stronger charge transfer state also leads to

an increase in the dipole moment of the excited state transition, which is beneficial for the improvement of fluorescence lifetime. (4) Adjusting the fatty amine chain altered the charge transfer process and π - π stacking, thereby affecting the solid-state luminescence. The unsatisfactory distance between surface-state monomers in aggregates will augment the non-radiative recombination, resulting in the PLQY varies non-monotonically with the length of the fatty amine chain. This work elucidates in depth the mechanism of carbon-core and surface-state luminescence in AIE CDs, revealing the chain length-regulated charge transfer and π - π stacking can engineer the solid-state emission wavelength, PLQY and AIE strength in CDs. It will provide guidance for achieving tunable wavelength emission and enhanced solid-state fluorescence.

4. Experimental Section

Material: Dithiosalicylic acid (DTSA), 1,5-diaminopentane, and 1,8-octanediamine were obtained from Energy Chemical Co. Ethylenediamine and 1,10-diaminodecane were purchased from Aladdin Shanghai, China. All the chemicals were used without further purification. Deionized (DI) water was used throughout the research.

Synthesis of Lx-CDs and Preparation of Nano-Aggregates: 245 mg of DTSA and 53 µL of ethylenediamine were sequentially added to a 50 mL beaker. Then, add acetic acid to the beaker and mix the raw materials evenly into a milky white cloudy liquid. Carefully transfer the white turbid liquid from the beaker to the hydrothermal kettle with the inner liner of polytetrafluoroethylene. Set the temperature of the blast drying oven to 180 °C, transfer the hydrothermal kettle to it after the temperature stabilizes, and react at this temperature for 10 h. Take a clear solution from the inner liner of polytetrafluoroethylene (hydrothermal kettle), add it to boiling water, stir to form a turbid solution, and then obtain purified CDs products through vacuum filtration, naming them L2-CDs. Ethylenediamine was replaced with 1,5-diaminopentane, 1,8-octenediamine, and 1,10-diaminodecane to prepare samples such as L5-CDs, L8-CDs, and L10-CDs.

Lx-CDs can be dispersed well in an acetic acid solution but not in water. Therefore, one chooses acetic acid as a good solvent for Lx-CDs and water as a poor solvent for Lx-CDs. First, prepare a 5 mg mL $^{-1}$ solution of Lx-CDs with acetic acid. Then, take 200 μL of Lx-CDs acetic acid solution and add an appropriate amount of water and acetic acid to prepare a 2 mL fixed volume test sample with a water ratio of 0%, 10%, 20%, 30%, 40%, 50%, 60%, 70%, 80%, and 90%, respectively.

Characterization: Transmission Electron Microscopy (TEM) was conducted using Talos F200X equipment to attain high-resolution imagery, which was set to function at an acceleration voltage of 200 kilovolts. Fourier Transform Infrared (FT-IR) Spectroscopy analyses were conducted utilizing a Bruker VERTEX70 device. Meanwhile, X-ray Photoelectron Spectroscopy (XPS) spectra were recorded via an ESCALAB Xi+ spectrometer. The equilibrium absorption and PL spectral characteristics of the specimens were measured employing a UV-2600 spectrophotometer for absorption and an FLS920 spectrophotometer (manufactured by Edinburgh Instruments) for PL. The PLQYs measurements were conducted using an FLS980 spectrometer from Edinburgh Instruments, which was equipped with an integrating sphere internally coated with polytetrafluoroethylene, and the samples were excited at a wavelength of 410 nm. The TCSPC technology was used to explore the TRPL of Lx-CDs.

Quantum Calculation and Molecular Dynamics Simulation: The quantum calculations were based on the Gaussian 09 program under the DFT and time-dependent (TD)-DFT.^[87–89] Concretely, the ground state for the optimization and excited properties involving charge-transfer excitation was carried out using CAM-B3LYP functional.^[90] The C, H, O, N, and S atoms were calculated using the 6–31G (d) basis set.^[91] The M06-2X method was implemented to optimize aggregates, including the multiple interactions.^[92] Gaussian Sum program^[93] was implemented to calculate the projected density of state (PDOS) of the molecular-specific

ADVANCED
OPTICAL
MATERIALS

21951071, 2025, 7, Downloaded from https://advanced.onlinelibrary.wiley.com/doi/10.1002/adom.202402638 by CAS-XIAN INSTITUTION OPTICS PRECISION MECHANICS, Wiley Online Library on [09/1/12025]. See the Terms and Conditions (https://activecom/doi/10.1002/adom.202402638 by CAS-XIAN INSTITUTION OPTICS PRECISION MECHANICS, Wiley Online Library on [09/1/12025]. See the Terms and Conditions (https://activecom/doi/10.1002/adom.202402638 by CAS-XIAN INSTITUTION OPTICS PRECISION MECHANICS, Wiley Online Library on [09/1/12025]. See the Terms and Conditions (https://activecom/doi/10.1002/adom.202402638 by CAS-XIAN INSTITUTION OPTICS PRECISION MECHANICS, Wiley Online Library on [09/1/12025]. See the Terms and Conditions (https://activecom/doi/10.1002/adom.202402638 by CAS-XIAN INSTITUTION OPTICS PRECISION MECHANICS, Wiley Online Library on [09/1/12025]. See the Terms and Conditions (https://activecom/doi/10.1002/adom.202402638 by CAS-XIAN INSTITUTION OPTICS PRECISION MECHANICS, Wiley Online Library on [09/1/12025]. See the Terms and Conditions (https://activecom/doi/10.1002/adom.202402638 by CAS-XIAN INSTITUTION OPTICS PRECISION MECHANICS, Wiley Online Library on [09/1/12025]. See the Terms and Conditions (https://activecom/doi/10.1002/adom.202402638 by CAS-XIAN INSTITUTION OPTICS PRECISION MECHANICS.

und-conditions) on Wiley Online Library for rules of use; OA articles are governed by the applicable Creative Commons License

contribution tendency to the highest occupied molecular orbital (HOMO) and the lowest unoccupied molecular orbital (LUMO) of the Lx-CDs. Finally, charge difference density (CDD) and charge transfer images were employed by the Multiwfn 3.6 program.^[94]

Molecular dynamics simulations constructed initial models for all studied aggregates. [45,95,96] Initially, crystal unit cells for the isolated molecules were generated using their optimized geometries. Subsequently, the stacking configurations were predicted employing the Dreiding force field, with the polymorph prediction calculations limited to ten space groups. The Particle Mesh Ewald method was utilized to compute the electrostatic interactions in aggregates. Following this, the initial energy minimization under 3D periodic boundary conditions allows for the prediction of the morphology of the research systems. The systems were then equilibrated using the canonical ensemble, followed by the isothermal-isobaric ensemble at a constant pressure of 1 bar and temperature of 300 K. Eventually, the geometric structures were optimized using quantum calculation.

Supporting Information

Supporting Information is available from the Wiley Online Library or from the author.

Acknowledgements

This work was supported by the National Natural Science Foundation of China (62027822 and 62175197), the National Key Research and Development Program of China (2019YFA0706402), the Natural Science Basic Research Program of Shaanxi Province of China (2018JM6012), and the Fundamental Research Funds for the Central Universities (xzy012019039).

Conflict of Interest

The authors declare no conflict of interest.

Data Availability Statement

The data that support the findings of this study are available in the supplementary material of this article.

Keywords

aggregation-induced emission (AIE), carbon dots (CDs), charge transfer, solid-state emission, π - π stacking

Received: September 29, 2024 Revised: December 9, 2024 Published online: January 16, 2025

- [1] C. L. Xia, S. J. Zhu, T. L. Feng, M. X. Yang, B. Yang, Adv. Sci. 2019, 6, 1901316.
- [2] M. J. Molaei, Anal. Methods 2020, 12, 1266.
- [3] J. K. Ren, H. Opoku, S. Tang, L. Edman, J. Wang, Adv. Sci. 2024, 11, 2405472.
- [4] C. L. Shen, Q. Lou, C. F. Lv, J. H. Zang, S. N. Qu, L. Dong, C. X. Shan, Adv. Sci. 2019, 6, 1802331.
- [5] H. X. Liu, X. Zhong, Q. Pan, Y. Zhang, W. T. Deng, G. Q. Zou, H. S. Hou, X. B. Ji, Coord. Chem. Rev. 2024, 498, 215468.
- [6] R. Fu, H. Q. Song, X. J. Liu, Y. Q. Zhang, G. J. Xiao, B. Zou, G. I. N. Waterhouse, S. Y. Lu, Chin. J. Chem. 2023, 41, 1007.

- [7] G. Z. Hu, Y. Wang, S. Zhang, H. Ding, Z. Y. Zhou, J. S. Wei, X. H. Li, H. M. Xiong, *Carbon* 2023, 203, 1.
- [8] W. Su, M. X. Tan, Z. H. Wang, J. Zhang, W. P. Huang, H. H. Song, X. Y. Wang, H. T. Ran, Y. F. Gao, G. J. Nie, H. Wang, Angewandte Chemie-International Edition 2023, 61, 202218128.
- [9] J. Li, H. Zhou, S. Jin, B. Xu, Q. Teng, C. H. Li, J. S. Li, Q. J. Li, Z. H. Gao, C. F. Zhu, Z. F. Wang, W. Su, F. L. Yuan, Adv. Mater. 2024, 36, 2401493.
- [10] J. Li, H. Zhou, H. Qiu, Y. Q. Yan, X. Wang, Z. H. Gao, Z. F. Wang, Coord. Chem. Rev. 2024, 503, 215642.
- [11] D. Y. Zhang, D. Y. Chao, C. Y. Yu, Q. Zhu, S. H. Zhou, L. Tian, L. Zhou, J. Phys. Chem. Lett. 2021, 12, 8939.
- [12] R. Y. Dai, X. P. Chen, N. Ouyang, Y. P. Hu, Chem. Eng. J. 2022, 431, 134172
- [13] J. L. Wang, J. X. Zheng, Y. Z. Yang, X. G. Liu, J. S. Qiu, Y. Tian, Carbon 2022, 190, 22.
- [14] C. L. Shen, Q. Lou, G. S. Zheng, M. Y. Wu, J. H. Zang, K. K. Liu, L. Dong, C. X. Shan, ACS Sustainable Chem. Eng. 2022, 10, 1624.
- [15] C. Wei, S. Hu, F. X. Liang, Z. N. Song, X. Liu, Chin. Chem. Lett. 2022, 33, 4116.
- [16] L. L. Tong, X. X. Wang, Z. Z. Chen, Y. H. Liang, Y. P. Yang, W. Gao, Z. H. Liu, B. Tang, Anal. Chem. 2020, 92, 6430.
- [17] W. H. Li, X. H. Wang, J. S. Lin, X. Y. Meng, L. H. Wang, M. R. Wang, Q. Jing, Y. Song, A. Vomiero, H. G. Zhao, *Nano Energy* **2024**, *122*, 109289.
- [18] M. Y. Cao, X. J. Zhao, X. Gong, Small 2022, 18, 2106683.
- [19] G. Eda, Y. Y. Lin, C. Mattevi, H. Yamaguchi, H. A. Chen, I. S. Chen, C. W. Chen, M. Chhowalla, Adv. Mater. 2010, 22, 505.
- [20] M. A. Sk, A. Ananthanarayanan, L. Huang, K. H. Lim, P. Chen, J. Mater. Chem. C 2014, 2, 6954.
- [21] N. Fuyuno, D. Kozawa, Y. Miyauchi, S. Mouri, R. Kitaura, H. Shinohara, T. Yasuda, N. Komatsu, K. Matsuda, Adv. Opt. Mater. 2014, 2 983
- [22] H. Ding, S. B. Yu, J. S. Wei, H. M. Xiong, ACS Nano 2016, 10, 484.
- [23] S. Ghosh, A. M. Chizhik, N. Karedla, M. O. Dekaliuk, I. Gregor, H. Schuhmann, M. Seibt, K. Bodensiek, I. A. T. Schaap, O. Schulz, A. P. Demchenko, J. Enderlein, A. I. Chizhik, *Nano Lett.* 2014, 14, 5656.
- [24] S. H. Jin, D. H. Kim, G. H. Jun, S. H. Hong, S. Jeon, ACS Nano 2013, 7, 1239.
- [25] Y. J. Zhang, R. R. Yuan, M. L. He, G. C. Hu, J. T. Jiang, T. Xu, L. Zhou, W. Chen, W. D. Xiang, X. J. Liang, *Nanoscale* 2017, 9, 17849.
- [26] M. J. Krysmann, A. Kelarakis, P. Dallas, E. P. Giannelis, J. Am. Chem. Soc. 2012, 134, 747.
- [27] V. Gude, A. Das, T. Chatterjee, P. K. Mandal, Phys. Chem. Chem. Phys. 2016, 18, 28274.
- [28] Z. A. Qiao, Q. S. Huo, M. F. Chi, G. M. Veith, A. J. Binder, S. A. Dai, Adv. Mater. 2012, 24, 6017.
- [29] S. J. Zhu, Y. B. Song, J. R. Shao, X. H. Zhao, B. Yang, Angewandte Chemie-International Edition 2015, 54, 14626.
- [30] Z. J. Zhou, P. F. Tian, X. Y. Liu, S. L. Mei, D. Zhou, D. Li, P. T. Jing, W. L. Zhang, R. Q. Guo, S. N. Qu, A. L. Rogach, Adv. Sci. 2018, 5, 1800369.
- [31] T. F. Liu, G. C. Yin, Z. Q. Song, J. K. Yu, X. Yong, B. W. Zhang, L. Ai, S. Y. Lu, ACS Mater. Lett. 2023, 5, 846.
- [32] Y. J. Wang, S. J. Zhou, S. M. Pan, X. F. Sun, J. Zhou, H. G. Li, Adv. Opt. Mater. 2024, 12, 2301486.
- [33] F. L. Yuan, T. Yuan, L. Z. Sui, Z. B. Wang, Z. F. Xi, Y. C. Li, X. H. Li, L. Z. Fan, Z. A. Tan, A. M. Chen, M. X. Jin, S. H. Yang, *Nat. Commun.* 2018. 9, 2249.
- [34] Z. B. Wang, N. Z. Jiang, M. L. Liu, R. D. Zhang, F. Huang, D. Q. Chen, Small 2021, 17, 2104551.
- [35] B. P. Jiang, Y. X. Yu, X. L. Guo, Z. Y. Ding, B. Zhou, H. Liang, X. C. Shen, *Carbon* 2018, 128, 12.
- [36] S. Y. Tao, S. Y. Lu, Y. J. Geng, S. J. Zhu, S. A. T. Redfern, Y. B. Song, T. L. Feng, W. Q. Xu, B. Yang, Angewandte Chemie-International Edition 2018, 57, 2393.



21951071, 2025, 7, Downloaded from https

://advanced.onlinelibrary.wiley.com/doi/10.1002/adom.202402638 by CAS-XIAN INSTITUTION OPTICS PRECISION MECHANICS, Wiley Online Library on [09/11/2025]. See the Terms and Conditions (https:

onditions) on Wiley Online Library for rules of use; OA articles are governed by the applicable Creative Commons I

- [37] B. Xu, J. Li, J. Zhang, H. Y. Ning, X. Q. Fang, J. Shen, H. Zhou, T. L. Jiang, Z. H. Gao, X. E. Meng, Z. F. Wang, Adv. Sci. 2023, 10, 2205788.
- [38] J. D. Luo, Z. L. Xie, J. W. Y. Lam, L. Cheng, H. Y. Chen, C. F. Qiu, H. S. Kwok, X. W. Zhan, Y. Q. Liu, D. B. Zhu, B. Z. Tang, Chem. Commun. 2001, 18, 1740.
- [39] Y. T. Lee, Y. T. Chang, C. T. Chen, C. T. Chen, J. Mater. Chem. C. 2016, 4, 7020.
- [40] M. Gao, B. Z. Tang, ACS Sens. 2017, 2, 1382.
- [41] L. Tang, L. Ai, Z. Q. Song, L. Z. Sui, J. K. Yu, X. Yang, H. Q. Song, B. W. Zhang, Y. S. Hu, Y. Q. Zhang, Y. X. Tian, S. Y. Lu, Adv. Funct. Mater. 2023, 33, 2303363.
- [42] Z. W. Guo, G. F. Li, H. Wang, J. Zhao, Y. H. Liu, H. W. Tan, X. P. Li, P. J. Stang, X. Z. Yan, J. Am. Chem. Soc. 2021, 143, 9215.
- [43] R. D. Crocker, D. P. Pace, B. L. Zhang, D. J. M. Lyons, M. M. Bhadbhade, W. W. H. Wong, B. K. Mai, T. V. Nguyen, J. Am. Chem. Soc. 2021, 143, 20384.
- [44] S. Suzuki, S. Sasaki, A. S. Sairi, R. Iwai, B. Tang, G. Konishi, Angewandte Chemie-International Edition 2020, 132, 9940.
- [45] Q. Y. Liao, Q. Q. Li, Z. Li, Adv. Mater. 2023, 2306617, https://doi.org/ 10.1002/adma.202306617.
- [46] R. Iwai, S. Suzuki, S. Sasaki, A. S. Sairi, K. Igawa, T. Suenobu, K. Morokuma, G. Konishi, Angewandte Chemie-International Edition **2020**, 59, 10566.
- [47] M. Y. Yu, Y. M. Guan, Q. X. Bai, P. Y. Su, P. S. Wang, T. Z. Xie, Adv. Opt. Mater. 2023, 11, 2202148.
- [48] H. Y. Yang, Y. L. Liu, Z. Y. Guo, B. F. Lei, J. L. Zhuang, X. J. Zhang, Z. M. Liu, C. F. Hu, Nat. Commun. 2019, 10, 1789.
- [49] X. K. Xu, L. Q. Mo, Y. D. Li, X. Q. Pan, G. Q. Hu, B. F. Lei, X. J. Zhang, M. T. Zheng, J. L. Zhuang, Y. L. Liu, C. F. Hu, Adv. Mater. 2021, 33,
- [50] Y. L. An, C. Liu, M. Chen, X. J. Yin, D. F. Hou, Y. W. Zheng, R. Shi, X. H. He, X. Lin, ACS Sustainable Chem. Eng. 2023, 11, 23.
- [51] C. Y. Ji, F. H. Zeng, W. J. Xu, M. J. Zhu, H. C. Yu, H. Yang, Z. L. Peng, Adv. Mater. 2024, 2414450. https://doi.org/10.1002/adma. 202414450.
- [52] X. F. Chen, W. X. Zhang, Q. J. Wang, Carbon 2014, 79, 165.
- [53] Y. S. Ma, X. M. Zhang, J. L. Bai, K. Huang, L. L. Ren, Chem. Eng. J. **2019**. *374*. 787.
- [54] J. C. Chen, H. G. Zhao, Z. L. Li, X. J. Zhao, X. Gong, Energy Environ. Sci. 2022, 15, 799.
- [55] Y. Song, C. Z. Zhu, J. H. Song, H. Li, D. Du, Y. H. Lin, ACS Appl. Mater. Interfaces 2017, 9, 7399.
- [56] J. L. He, Y. L. He, Y. H. Chen, B. F. Lei, J. L. Zhuang, Y. Xiao, Y. R. Liang, M. T. Zheng, H. R. Zhang, Y. L. Liu, Small 2017, 13, 1700075.
- [57] Y. H. Chen, M. T. Zheng, Y. Xiao, H. W. Dong, H. R. Zhang, J. L. Zhuang, H. Hu, B. F. Lei, Y. L. Liu, Adv. Mater. 2016, 28, 312.
- [58] R. Y. Cong, X. N. He, S. L. Zhao, W. Gao, H. Li, S. J. Liang, M. Liu, J. H. Zhang, J. Appl. Polym. Sci. 2022, 139, e53151.
- [59] H. X. Li, D. D. Su, H. Gao, X. Yan, D. S. Kong, R. Jin, X. M. Liu, C. G. Wang, G. Y. Lu, Anal. Chem. 2020, 92, 3198.
- [60] X. J. Fu, G. Q. Li, S. Y. Cai, H. Yang, K. Lin, M. He, J. W. Wen, H. B. Li, Y. B. Xiong, D. Z. Chen, X. H. Liu, Carbohydr. Polym. 2021, 251, 117084.
- [61] Y. S. Liu, H. Y. Yang, Y. Wang, C. H. Ma, S. Luo, Z. W. Wu, Z. S. Zhang, W. Li, S. X. Liu, Chem. Eng. J. 2021, 424, 130426.
- [62] Y. Q. Zhang, X. Y. Liu, Y. Fan, X. Y. Guo, L. Zhou, Y. Lv, J. Lin, Nanoscale **2016**, 8, 15281.
- [63] S. E. Wheeler, J. W. G. Bloom, J. Phys. Chem. A. 2014, 118, 6133.
- [64] T. Y. Zhou, T. T. Li, J. Y. Hou, Y. B. Wang, B. Hu, D. S. Sun, Y. Y. Wu, W. Jiang, G. B. Che, C. B. Liu, Chem. Eng. J. 2022, 445, 136643.

- [65] G. G. B. Alves, A. Batagin-Neto, J. Phys. Chem. C. 2023, 127, 3819.
- [66] J. S. Murray, P. Politzer, Wiley Interdisciplinary Reviews-Computational Molecular Science 2011, 1, 153.
- [67] Y. M. Luo, Q. Jiang, J. K. Liu, H. W. Yang, X. L. Liao, F. Y. Huang, J. L. Zhuang, C. F. Hu, B. F. Lei, Y. L. Liu, J. L. He, Chem. Eng. J. 2024, 486, 150436.
- [68] X. T. Wang, Q. L. Zhao, Q. H. Song, H. Bu, J. Gao, L. L. Li, X. F. Yu, X. J. Yang, Z. M. Lu, X. H. Zhang, Spectrochimica Acta Part A-Molecular And Biomolecular Spectroscopy 2024, 310, 123952.
- [69] K. Holá, M. Sudolská, S. Kalytchuk, D. Nachtigallová, A. L. Rogach, M. Otyepka, R. Zboril, ACS Nano 2017, 11, 12402.
- [70] H. El-Gezawy, W. Rettig, Chem. Phys. 2006, 327, 385.
- [71] X. B. Fan, W. C. Peng, Y. Li, X. Y. Li, S. L. Wang, G. L. Zhang, F. B. Zhang, Adv. Mater. 2008, 20, 4490.
- [72] T. Le Bahers, T. Pauporté, G. Scalmani, C. Adamo, I. Ciofini, T. Pauporté, G. Scalmani, C. Adamo, I. Ciofini, Phys. Chem. Chem. Phys. **2009**, 11, 11276.
- [73] R. A. Marcus, Annu. Rev. Phys. Chem. 1964, 15, 155.
- [74] R. A. Marcus, Rev. Mod. Phys. 1993, 65, 599.
- [75] Acc. Chem. Res. 2013, 46, 1144.
- [76] R. J. Cave, M. D. Newton, Chem. Phys. Lett. 1996, 249, 15.
- [77] P. Kjellberg, Z. He, T. Pullerits, J. Phys. Chem. B. 2003, 107, 13737.
- [78] M. E. Köse, K. S. Schanze, J. Phys. Chem. A. 2020, 124, 9478.
- [79] H. F. Zhao, H. Yin, X. C. Liu, H. Li, Y. Shi, C. L. Liu, M. X. Jin, J. B. Gao, Y. Luo, D. J. Ding, J. Phys. Chem. Lett. 2019, 10, 3064.
- [80] F. G. Shen, A. D. Peng, Y. Chen, Y. Dong, Z. W. Jiang, Y. B. Wang, H. B. Fu, J. N. Yao, J. Phys. Chem. A. 2008, 112, 2206.
- [81] Y. H. Deng, X. J. Feng, D. J. Yang, C. H. Yi, BioResources 2022, 7, 1145.
- [82] L. P. Yang, Y. L. Song, G. H. Fan, X. R. Zhang, Y. X. Wang, Spectrochimica Acta Part A-Molecular and Biomolecular Spectroscopy 2021, 259, 119830.
- [83] J. F. Gonthier, S. N. Steinmann, L. Roch, A. Ruggi, N. Luisier, K. Severin, C. Corminboeuf, Chem. Commun. 2012, 48, 9239.
- [84] B. Zhao, H. Ma, H. Y. Jia, M. Y. Zheng, K. X. Xu, R. N. Yu, S. N. Qu, Z. A. Tan, Angewandte Chemie-International Edition 2023, 62, 202301651.
- [85] T. Lu, Q. X. Chen, Chemistrymethods 2021, 1, 231.
- E. R. Johnson, S. Keinan, P. Mori-Sánchez, J. Contreras-García, A. J. Cohen, W. T. Yang, J. Am. Chem. Soc. 2010, 132, 6498.
- R. Misra, R. Maragani, D. Arora, A. Sharma, G. D. Sharma, Dyes Pigm. [87] 2016, 126, 38.
- S. Ashraf, E. Yildirim, J. Akhtar, H. M. Siddiqi, A. El-Shafei, Phys. [88] Chem. Chem. Phys. 2017, 19, 20847.
- [89] M. J. Frisch, G. W. Trucks, H. B. Schlegel, G. E. Scuseria, M. A. Robb, J. R. Cheeseman, G. Scalmani, V. Barone, B. Mennucci, G. A. Petersson, H. Nakatsuji, M. Caricato, X. Li, H. P. Hratchian, A. F. Izmaylov, J. Bloino, G. Zheng, J. L. Sonnenberg, M. Hada, M. Ehara, K. Toyota, R. Fukuda, J. Hasegawa, M. Ishida, T. Nakajima, Y. Honda, O. Kitao, H. Nakai, T. Vreven, J. A. Montgomery Jr, et al., Gaussian 09, Gaussian, Inc., Wallingford, CT, USA 2009.
- [90] T. Yanai, D. P. Tew, N. C. Handy, Chem. Phys. Lett. 2004, 393, 51.
- [91] J. Mol. Struct. 2017, 1127, 694.
- [92] Y. Zhao, D. G. Truhlar, Theor. Chem. Acc. 2008, 120, 215.
- [93] B. Nagarajan, S. Kushwaha, R. Elumalai, S. Mandal, K. Ramanujam, D. Raghavachari, J. Mater. Chem. A. 2017, 5, 10289.
- [94] T. Lu, F. W. Chen, J. Comput. Chem. 2012, 33, 580.
- [95] G. Guo, Y. S. Xia, Anal. Chem. 2024, 96, 5095.
- [96] L. Ai, Y. F. Pei, Z. Q. Song, X. Yong, H. Q. Song, G. J. Liu, M. J. Nie, G. I. N. Waterhouse, X. B. Yan, S. Y. Lu, Angew. Chem. 2023, 135, 202217822.